Synergistic use of ground-based GNSS-R and Sentinel-2 imagery for soil moisture estimation across an irrigated grassland

El Hajj, Marcel M.; Steele-Dunne, Susan C.; Johansen, Kasper; Almashharawi, Samer K.; Lopez Valencia, Oliver M.; Lopez Camargo, Omar A.; Amezaga-Sarries, Adria; Mas-Viñolas, Andreu; Courault, Dominique; Doussan, Claude

DOI
10.1109/TGRS.2025.3555000

Publication date
2025

Document Version
Final published version

Published in
IEEE Transactions on Geoscience and Remote Sensing

Synergistic Use of Ground-Based GNSS-R and Sentinel-2 Imagery for Soil Moisture Estimation Across an Irrigated Grassland

Marcel M. El Hajj, Susan C. Steele-Dunne, *Member, IEEE*, Kasper Johansen, Samer K. Almashharawi, Oliver M. Lopez Valencia, Omar A. López Camargo, *Student Member, IEEE*, Adria Amezaga-Sarries, Andreu Mas-Viñolas, Dominique Courault, Claude Doussan, and Matthew F. McCabe

***Abstract*— Soil moisture (SM) plays a central role in water cycle dynamics and land–atmosphere interactions, acting across local and regional scales. Few studies have explored the use of the ground-based global navigation satellite system reflectometry (GNSS-R) interference pattern technique (IPT) for SM estimation. In these studies, SM was estimated from the GPS elevation angle where lower reflectivity occurs (notch), which is difficult to determine in real GNSS-R interference power (IP) acquisitions. This study introduces the use of IP amplitude at vertical polarization (V-pol), readily extracted from the IP oscillations, as an alternative for SM estimation beneath vegetation cover. An empirical model was developed for estimating SM in irrigated grassland using a GNSS-R receiver with a linearly polarized antenna. The experiment, conducted between June 6 and August 8, 2022, covered the grassland's growth phase and preharvesting and postharvesting. The study incorporated normalized difference water index (NDWI) from the Sentinel-2 satellite to account for vegetation's impact on IP amplitude. Results indicated that the IP amplitude at V-pol accurately estimates SM (RMSE = 0.04 m^3/m^3). Moreover, the results show that the vegetation layer mainly attenuates the IP amplitude with a nonsignificant scattered contribution to the IP, allowing for the simplification of the empirical model by ignoring the scattered contribution of vegetation. The simplified empirical model can be numerically resolved to estimate the NDWI if the SM is known. In summary, this study highlights the effectiveness of the ground-based IPT for close-range sensing of SM and a biomass proxy, such as NDWI.**

***Index Terms*— Global navigation satellite system reflectometry (GNSS-R), interference power (IP), normalized differential water index, soil moisture (SM).**

Received 30 June 2024; revised 6 February 2025; accepted 18 March 2025. Date of publication 27 March 2025; date of current version 22 April 2025. This work was supported by the King Abdullah University of Science and Technology. *(Corresponding author: Marcel M. El Hajj.)*

Marcel M. El Hajj, Kasper Johansen, Samer K. Almashharawi, Oliver M. Lopez Valencia, Omar A. López Camargo, and Matthew F. McCabe are with the Hydrology, Agriculture and Land Observation (HALO) Laboratory, Division of Biological and Environmental Sciences and Engineering, King Abdullah University of Science and Technology (KAUST), Thuwal 23955, Saudi Arabia (e-mail: marcel.elhajj@kaust.edu.sa).

Susan C. Steele-Dunne is with the Department of Geoscience and Remote Sensing, Delft University of Technology, 2628 Delft, The Netherlands.

Adria Amezaga-Sarries and Andreu Mas-Viñolas are with Microwave Sensors and Electronics SL, 08720 Barcelona, Spain.

Dominique Courault and Claude Doussan are with UMR 1114 EMMAH INRAE, Avignon University, 84914 Avignon, France.

Digital Object Identifier 10.1109/TGRS.2025.3555000

I. Introduction

CONTINUOUS monitoring of soil moisture (SM) in areas with both bare soil and vegetation cover is of value across numerous applications, from validating land surface models and improving our understanding of weather and climate processes, to enhancing the description of hydrological response and agricultural management [1], [2]. For instance, repetitive SM information used to derive initial and boundary conditions improves hydrological model predictions and reduces the uncertainties involved in the prediction process [3]. In addition, monitoring SM in agricultural areas is vital for guiding irrigation practices, alerting farmers to potential deficits in SM below the wilting point, and optimizing yield and averting crop damage [4], [5]. Synthetic aperture radar (SAR) is one technique that has been used for remote retrieval of SM at agricultural plot scales and larger [6]. In particular, Sentinel-1 (C band), which is the only current SAR satellite freely available at high resolution (10 × 10 m) and high revisit time (up to six days), has shown considerable potential for repetitive SM mapping over small agricultural plots [6]. However, the C band cannot sense SM underneath a well-developed vegetation cover due to the limited penetration depth of the emitted wave in the canopy, thereby preventing SM monitoring during the maturity stage [7]. In addition, the use of current SAR images cannot provide the required revisit time (daily or subdaily) for effective irrigation management, highlighting the need for additional retrieval techniques and approaches.

Over the past decade, global navigation satellite system reflectometry (GNSS-R) has emerged as a "signal of opportunity" [8] for continuous and near real-time SM and vegetation parameter estimation at a subplot scale [9]. With ground-based GNSS-R, the estimation of SM is based on the use of the direct signal from GNSS satellites and the reflected signal from the Earth's surface [9], [10], [11]. Most studies have employed an interferometric GNSS-R ground-based receiver with a single antenna to estimate SM and vegetation parameters by analyzing the phase, amplitude, and frequency of the signal-to-noise ratio (SNR) waveform [9]. In GNSS-IR antennas, the interference between the direct and reflected signal is observed in temporal variations of the SNR waveform [10],

[12]. The interference pattern technique (IPT) was introduced in 2009 by Rodriguez-Alvarez et al. [11] as an alternative means to estimate SM. A unique feature of the IPT approach is that it measures the power fluctuations of the interference of the direct and the reflected signals as a function of the GNSS satellite elevation angle. This allows the use of information on the satellite elevation angle for SM and vegetation parameter estimation from the interference power (IP) waveform at vertical polarization. For instance, Rodriguez-Alvarez et al. [11] estimated the SM of bare soil from the so-called notch position, which is the satellite angular elevation value of the smallest IP oscillation at vertical polarization. As the determination of the notch position is not straightforward [13], a recent study by El Hajj et al. [14] presented a practical approach to estimate SM over bare smooth soil by using the coefficient of determination between the IP at horizontal (H-pol) and vertical (V-pol) polarizations as a predictor of SM. This method yielded accurate estimates of SM in bare soil (sand 78%, silt 10%, and clay 12%) at 10 cm in depth, with a root-mean-square error (RMSE) of approximately 1.5 vol%.

To the best of our knowledge, there is only one study [15] that used IP oscillation from IPT to estimate SM and vegetation height, with that investigation focusing on tracking the wheat through a growing season (heights between 10 and 60 cm). In that study [15], SM and wheat height were estimated by determining the position of multiple notch positions in the IP oscillation for satellite elevation values between 5 and 70. To determine the notch positions, Rodriguez-Alvarez et al. [15] computed the upper and lower envelopes of the IP waveform at V-pol, with the notch position being where the difference between the upper and lower envelopes was the smallest. Several studies [11], [13], [14] found it challenging to accurately determine notch positions in real GNSS-R acquisitions, especially when the IP oscillation exhibits low-frequency oscillations or maintains a constant amplitude over a wide range of satellite elevation angles. Therefore, a more robust and practical method to estimate SM from IP waveforms over vegetated areas is needed.

In general, two kinds of GNSS-R data inversion approaches have been applied to estimate SM and vegetation parameters: 1) the development of an empirical relationship between GNSS-R and in situ data and 2) the use of a physical model to invert the GNSS-R data. For example, Rodriguez-Alvarez et al. [15] utilized a full electromagnetic model to establish the relationships between the number of notches and medium parameters and employed these relationships to estimate SM and wheat height from GNSS-R IP oscillations. Similarly, El Hajj et al. [14] first used the coherent specular reflection model [16] to establish the relation between SM and the coefficient of determination between IP at H-pol and V-pol, with this relationship then applied to estimate SM from the coefficient of determination obtained from GNSS-R acquisitions over a bare smooth soil.

In the presence of vegetation cover, using a physical model, such as the coherent specular reflection model [16], to estimate SM is complex. While physical models can be used in the simulation step to relate GNSS-R signals to various soil and vegetation parameters, their use in inversion schemes to estimate the SM requires input vegetation parameters that are not routinely available, such as water content, height, and plant structure [15], [17], [18]. In this context, the use of the empirical approach facilitates the estimation of soil and vegetation parameters by providing the possibility to reduce the number of vegetation parameters required to describe the canopy and enabling the use of vegetation descriptor indices more readily obtained from remote sensing data [e.g., the normalized difference vegetation index (NDVI) and normalized difference water index (NDWI)].

Given this context, the main objective of this study is to develop an empirical approach that can infer the SM underneath a vegetated grassland surface using GNSS-R signals. To do this, the vertical component of the interference pattern was recorded by a ground-based GPS receiver, i.e., the SM interference-pattern GNSS observations at L-band reflectometer (SMIGOL-R), which was installed within an irrigated grassland field during one growth cycle. The SMIGOL-R-derived SM estimates were validated against in situ SM measurements collected between June 6 and August 8, 2022. Through estimating SM on bare and vegetated soil covers from a network of ground-based GNSS-R, we can obtain useful information for the calibration and validation process of current and future satellite missions aimed at monitoring SM at a regional to global scale. Furthermore, frequent SM estimation using GNSS-R in agricultural areas can provide insights into understanding the dynamics of SM in relation to the irrigation calendar, thus allowing for the optimization of irrigation activities.

II. Dataset Collection

A. SMIGOL-R and Related In Situ Data

The study was conducted in a grassland field (silty soil) of approximately 3 h in southern France (5.013185°, 43.644 067°), which was being used for hay production [19]. The field is leveled and irrigated through the overflow of a canal (border irrigation), which brings water from upstream to downstream across the field surface by gravity (Fig. 1). The border irrigation system ensures even water distribution within the plot and resulting in more homogenous SM compared to a nonirrigated or otherwise unfarmed field. Irrigation is applied, on average, every ten days between March and October, and the field is harvested three times a year. This field was selected because it exhibits large variations in SM and biomass due to frequent border irrigation and machine harvest at the end of each growth cycle.

The SMIGOL-R was positioned at a height of 4.75 m within the grassland site. The SMIGOL-R antenna was oriented horizontally at an azimuth angle of approximately 220° to avoid reflection from tall trees located along the edge of the field (Fig. 1). A weather station was installed in the field to gather standard meteorological data along with SM measurements at a depth of 7 cm, using two calibrated Stevens HydraProbe-II sensors with a measurement rate of 1 min. These sensors were horizontally installed 50 cm apart at a 7 cm depth to avoid the measurement volume extending into

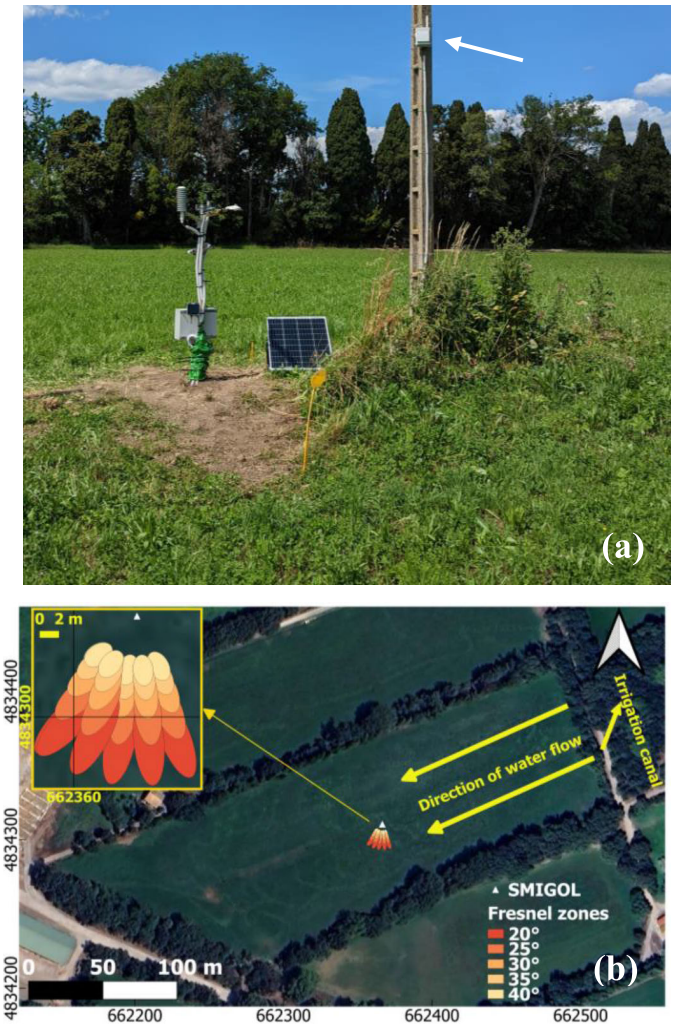

Fig. 1. (a) SMIGOL-R receiver installed at a height of 4.75 m, together with the solar power supply and collocated weather station. (b) Aerial photograph showing the location of the SMIGOL-R within the grassland field, with ellipses representing the calculated Fresnel zones, as an example, for GPS number 73 orbiting between elevation angles of 20° and 40° and azimuth angles of 158° and 227°, considering an antenna height of 4.75 m. *X*- and *Y*-axis coordinates are in UTM 31N.

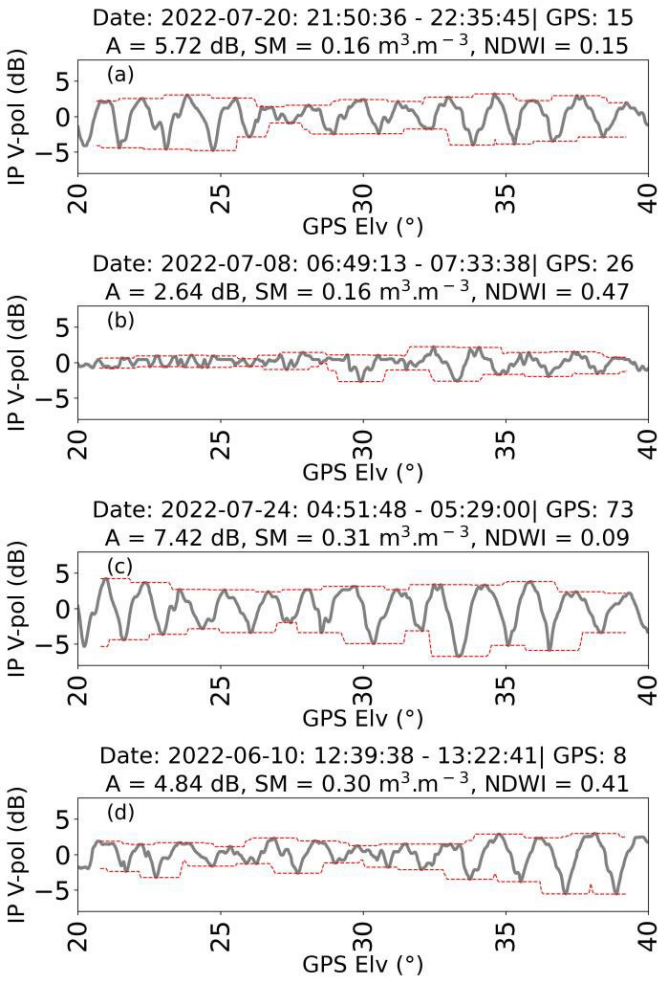

Fig. 2. IP oscillations according to GPS elevation angle for different SM and NDWI conditions. (a) Low SM and NDWI. (b) Low SM and high NDWI. (c) High SM and low NDWI. (d) High SM and NDWI. Titles show acquisition date, time (start and end), GPS number, IP amplitude (A), soil moisture, and NDWI values. Red lines show the upper and lower envelopes of IP oscillations.

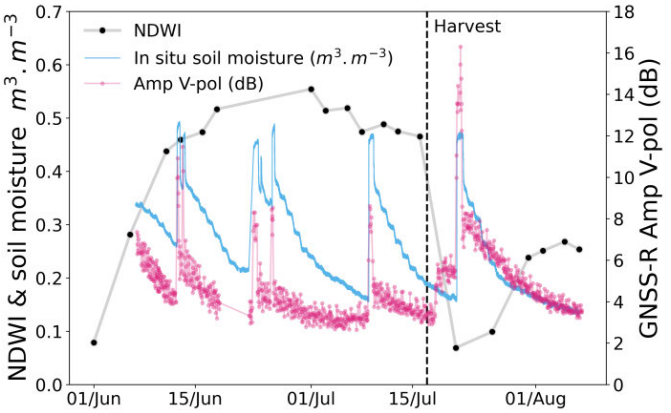

Fig. 3. Temporal variations of NDWI, SM, and GNSS-R IP amplitude throughout the experiment.

the air above the surface. The Stevens HydraProbe-II sensors were located ∼7 m away from—and directly in front of—the antenna's orientation. Measurements from the two SM sensors were averaged to represent the SM within the SMIGOL-R footprint (Fig. 1). Meteorological and SM data were collected throughout the SMIGOL-R acquisition period, covering from June 6 to August 8, 2022. SM measurements show that after each irrigation event (frequency of 8–10 days), the SM reaches approximately 0.48 $m^3 \cdot m^{-3}$ and then gradually decreases over time until the next irrigation event (Fig. 3). The longer the interval between the irrigation events, the lower the SM values before the next irrigation (Fig. 3). The high value of SM during irrigation (0.48 $m^3 \cdot m^{-3}$) is related to the flooding irrigation practice of the grassland, which induces a ponding depth of up to 5 cm at the soil surface. The grass growth restarted on June 1 after the previous cut, and the field was harvested on July 17. As such, the GNSS-R acquisitions cover the majority of the growth cycle, plus an additional 21 days postharvest. Vegetation height measurements were conducted preharvest on July 6, recording a grass height of approximately 90 cm. In a previous study, Hajj et al. [19] conducted intensive field measurements over the same site and demonstrated that before harvest, the fresh biomass and leaf area index of the vegetation reached values of approximately 4 kg/m^2 and 4.5 m^2/m^2,

respectively. The soil roughness of the plot is approximately 0.7 cm [19].

The SMIGOL-R system, developed by Microwave Sensors and Electronics (https://www·mwse.tech/), measures the instantaneous IP at V-pol from both direct and reflected GPS L1-band signals (1.57 542 GHz). It operates by capturing the IP variations as GPS satellites move. Thus, the recorded IP is a function of satellite elevation angle. The reflected signals originate from the Fresnel zone, an elliptical area surrounding the specular point, where scattered signals with a normalized scattering coefficient higher than 1/e are collected [11]. The dimensions of the Fresnel zone are determined by factors such as antenna height, soil roughness, and satellite elevation angle. The antenna pattern corresponds to one of a single patch, so the beamwidth (−3 dB) of around 70°–80° is symmetrical. Further details about the antenna can be found in [11] and [14].

B. Sentinel 2 Optical Data

The GNSS-R reflected signal is affected by the presence of vegetation cover [20], [21]. To model the effect of vegetation on the GNSS-R signal, several studies have used parameters such as plant water content and canopy structure [15], [17], [18], [22]. As measuring these quantities is labor-intensive and time-consuming, vegetation metrics were obtained from Sentinel-2 images at the plot scale. In this case, the NDWI, which is commonly used to monitor changes in water content [23], [24], was employed as a descriptor of vegetation development. Indeed, it is known that the vegetation water content is the dominant effect on the L-band signal, playing a much larger role than other plant elements such as the main stem [21]. Here, the NDWI (average value over the Fresnel zone) was derived from 19 cloud-free Sentinel-2 images collected between June 1 and August 8, 2022, using the near-infrared (NIR) and shortwave infrared (SWIR) bands as follows:

$$\mathrm{NDWI} = \frac{\mathrm{NIR} - \mathrm{SWIR}}{\mathrm{NIR} + \mathrm{SWIR}}. \tag{1}$$

Estimating SM from each GNSS-R acquisition requires coincident NDWI values, a task impeded by the revisit time of Sentinel-2 (up to two days with Sentinel-2 orbits 8 and 108 over the study site) and the presence of clouds. In this study, linear interpolation of NDWI was performed using cloud-free Sentinel-2 images to obtain a daily NDWI value, with the NDWI value considered equal for all GNSS-R acquisitions within a day. Fig. 3 shows the temporal variations of NDWI between June 1 and August 8. Results show that the NDWI increases rapidly from June 1 to reach a maximum on July 1 (NDWI = 0.55). It decreases slightly between July 1 and July 9 (NDWI = 0.48) and remains constant until the harvest on July 17. After harvest, the NDWI was 0.07 followed by a rapid increase due to vegetation growth.

III. Methodology

The study aims to provide an empirical model for estimating SM while considering the impact of vegetation development on the IP oscillation recorded by the SMIGOL-R receiver. As the notch position (the more common variable used in SMIGOL studies) is not straightforward to retrieve, an alternative predictor of SM that can be easily computed from the IP oscillation must be considered. A potential candidate predictor is the IP amplitude, which is the mean of the difference between the upper and lower envelopes of IP oscillation as a function of the satellite elevation angle. Studies have shown that for a given range of satellite elevation angles, the amplitude of IP oscillation at V-pol increases with increasing SM [11], [13], [14]. However, the relationship between IP amplitude at V-pol and SM in the presence of vegetation remains unknown, as it has not been explored in previous research.

Based on the theory of L-band interactions with vegetation cover, the IP amplitude is a function of both vegetation and SM scattering, with the SM contribution being attenuated by the presence of vegetation [14], [15], [21]. Accordingly, the IP amplitude (A) can be empirically expressed as a function of soil and vegetation according to the following equation:

$$A = a * \mathrm{NDWI} * \left(1 - e^{-b*\mathrm{NDWI}}\right) + c * \mathrm{SM}^d * e^{-b*\mathrm{NDWI}} \tag{2}$$

where A is the GNSS-R IP amplitude, i.e., the mean of the difference between the upper and lower envelopes of IP oscillation within a range of satellite elevation angles, for a given polarization in linear units [25]. The term $[a * \mathrm{NDWI}]$ represents the vegetation scattering, which accounts for the IP amplitude increase (enhanced contribution) due to the presence of water within the vegetation [21]. The term $[c * \mathrm{SM}^d * e^{-b*\mathrm{NDWI}}]$ accounts for the SM scattering (i.e., $[c * \mathrm{SM}^d]$) attenuated by the NDWI when multiplied by $[e^{-b*\mathrm{NDWI}}]$, causing an exponential decrease in GNSS-R IP amplitude (A). The term $[1 - e^{-b*\mathrm{NDWI}}]$ accounts for the remaining part of the attenuation by the vegetation. For instance, when the vegetation is low (NDWI ∼0), the term $[a*\mathrm{NDWI}*(1-e^{-b*\mathrm{NDWI}})]$ becomes equal to 0 (no vegetation contribution) and the term $[c*\mathrm{SM}^d*e^{-b*\mathrm{NDWI}}]$ becomes equal to $[c*\mathrm{SM}^d]$, leading to the expression of IP amplitude (A) as a function of SM only. The fitting parameters a, b, c, and d need to be estimated for each polarization through calibration using the GNSS-R measurements, Sentinel-2 derived NDWI, and recorded in situ SM.

Equation (2) was formulated based on the theory of GNSS-R signal interactions with SM beneath developing vegetation cover [15], [20], [21]. However, to determine its applicability, the formulation requires validation using the experimental data collected herein (GNSS-R, NDWI, and in situ SM), as the variation of IP amplitude according to SM beneath changing vegetation conditions has not been explored in previous research. Therefore, the relationship between IP amplitude and SM was examined based on the experimental data for three different ranges of NDWI values (NDWI ≤ 0.3, $0.3 < \mathrm{NDWI} \leq 0.5$, and NDWI > 0.5), aiming to minimize the influence of vegetation cover on the IP variations according to SM. The results from the experimental analysis should reflect the behavior of the IP amplitude according to the expected SM and NDWI values based on (2).

The proposed empirical model [see (2)] requires calibration (i.e., estimation of constants a, b, c, and d) in order to be used for SM estimation. To avoid overfitting, the dataset was split

into two quasi-equal parts, with one used for calibration and the other for validation of the calibration and SM estimation. It is important that the part used for calibration covers the full range of SM and NDWI conditions encountered during the experiment. To split the dataset, it was divided into six parts so that each part contains a given range of NDWI: NDWI $\leq$ 0.1, 0.1 < NDWI $\leq$ 0.2, 0.2 < NDWI $\leq$ 0.3, 0.3 < NDWI $\leq$ 0.4, 0.4 < NDWI $\leq$ 0.5, and NDWI > 0.5. Then, from each part, one row (containing IP amplitude and the corresponding SM and NDWI) was selected for the calibration dataset and one row was selected for the validation dataset, taken from every two consecutive rows. The corresponding SM for a given IP amplitude was the average of 1-min SM measurements recorded during that IP acquisition. All rows selected for calibration were concatenated to form the calibration dataset. Similarly, all rows selected for validation were concatenated to form the validation dataset.

The Levenberg–Marquardt method was used to estimate the empirical model parameters (a, b, c, and d) from the calibration dataset. To determine the accuracy of model calibration, the calibrated empirical model [see (2)] was used to estimate the IP amplitude from SM and NDWI of the validation dataset. The estimated IP amplitude was then compared to that measured by the SMIGOL-R. The accuracy of the calibration was quantified using the RMSE, bias (estimated – measured), and coefficient of determination (R^2). The SM was then estimated by inverting the calibrated empirical model [see (2)] using the validation dataset and compared to the in situ SM via RMSE, bias, and R^2.

IV. Results and Discussion

A. Sensitivity of GNSS-R Amplitude to SM and NDWI

To understand the contribution of SM and vegetation to the IP amplitude, we examined the variation of the IP amplitude in relation to SM and NDWI. In this study, the IP oscillation was only considered between elevation angles of 20° and 40° because the signal is deteriorated at lower elevation angles due to the signal occlusion by the tall trees present along the plot perimeters. Four representative cases of IP oscillations were analyzed for "dry" soil conditions of the irrigated grassland field (0.16 $m^3 \cdot m^{-3}$) (Fig. 3) with low (0.15) and high (0.47) NDWI values [Fig. 2(a) and (b)], and for "wet" soil conditions (0.30 $m^3 \cdot m^{-3}$) with low (0.09) and high (0.41) NDWI values [Fig. 2(c) and (d)]. Results show that for similar SM conditions, the amplitude of the IP oscillations is lower for high NDWI values, indicating that the presence of vegetation attenuates the amplitude of the IP (Fig. 2) [20], [21]. For instance, for SM of 0.16 $m^3 \cdot m^{-3}$, the IP amplitude was 5.72 and 2.64 dB for NDWI of 0.15 and 0.47, respectively. Most importantly, Fig. 2 shows that the IP amplitude increases with increasing SM even when the NDWI is high, illustrating that the sensitivity to SM is significant at high NDWI values. For instance, for a high NDWI value (NDWI = 0.47), the IP amplitude increases from 2.64 to 4.84 dB as the SM increases from 0.16 to 0.30 $m^3 \cdot m^{-3}$ [Fig. 2(b) and (d)].

The temporal variation of IP at V-pol was analyzed along with those of SM and NDWI for the entire experiment period (Fig. 3). Results show that the IP amplitude covaries with SM and the sensitivity of IP amplitude variations to SM is higher when the NDWI values are low. These findings indicate that the vegetation attenuates the contribution of SM to the IP amplitude. For instance, between June 24 and July 7 (NDWI > 0.45), the IP amplitude decreases by approximately 1.2 dB (from 4.2 to 3.0 dB) when SM decreases 0.19 $m^3 \cdot m^{-3}$ (from 0.35 to 0.16 $m^3 \cdot m^{-3}$), yielding a sensitivity of 6.32 $dB/m^3 \cdot m^{-3}$. Conversely, in lower vegetation water conditions (NDWI < 0.28), between July 21 and August 8, the IP amplitude decreases by approximately 4.2 dB (from 7.9 to 3.7 dB) when SM decreases 0.14 $m^3 \cdot m^{-3}$ (from 0.26 to 0.12 $m^3 \cdot m^{-3}$), yielding a sensitivity of 30 $dB/m^3 \cdot m^{-3}$. When the plot was completely machine-harvested on July 17, the IP amplitude quickly increased by 2.5 dB, confirming that the presence of vegetation attenuates the IP amplitude. Unfortunately, the harvested biomass was not known, making it impossible to calculate the change in IP amplitude associated with this abrupt biomass change. The decrease in IP value due to harvest is a good estimator of biomass level, especially when the harvest occurs within a short time frame during which the SM does not significantly change, making the decrease in IP exclusively related to the biomass change. Future research should focus on building a relationship between changes in IP value and biomass.

In addition to the sensitivity of IP amplitude to SM, Fig. 3 shows a large increase in the IP amplitude during irrigation. This large increase is caused by the higher reflectivity of the ponded surface water layer. Water's electric permittivity constant is approximately 80, while that of the air is 1.0006. When a GPS signal travels through a low permittivity medium (i.e., the grass layer) and encounters a high permittivity medium (i.e., irrigation water), its reflectivity index approaches one, indicating that most of the signal bounces back to the first medium with minimal energy loss. For this reason, the reflected signal reaching the receiver is much higher for the ponded surface water compared to other SM conditions, producing a higher IP amplitude. Data influenced by these increases in IP amplitude were not used in further analysis as the GNSS-R emitted signal is reflected from the ponded surface water layer and not from the soil. However, it is worth noting that the double-bounce amplitude is lower when the NDWI is high compared to when the NDWI is low, confirming the attenuation of IP amplitude by the vegetation. For instance, the double-bounce IP amplitude is approximately 16 dB when the NDWI was 0.07 (on July 21), compared to 8 dB when the NDVI was 0.48 (on July 10).

The correlation between IP amplitude and SM was analyzed for different ranges of NDWI to assess the vegetation effects on the correlation (Fig. 4). Results show that the IP amplitude is correlated to the SM with higher sensitivity for low NDWI values. The sensitivity of IP amplitude to SM was 19.45 $dB/m^3 \cdot m^{-3}$ ($R^2 = 0.88$) for NDWI $\leq$ 0.3, 9.36 $dB/m3 \cdot m^{-3}$ ($R^2 = 0.61$) for NDWI between 0.3 and 0.5, and 5.83 $dB/m^3 \cdot m^{-3}$ ($R^2 = 0.55$) for NDWI > 0.5. Fig. 4 also shows that for a given value of SM, the IP amplitude decreases as the NDWI increases due to the increase in attenuation by the grass.

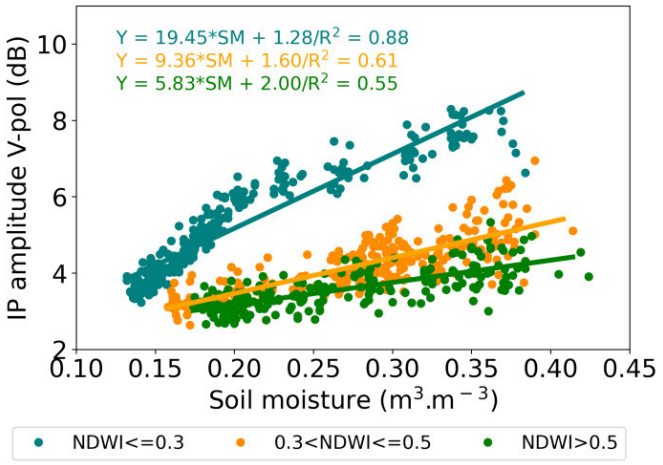

Fig. 4. Correlation between IP amplitude and SM for different ranges of NDWI values.

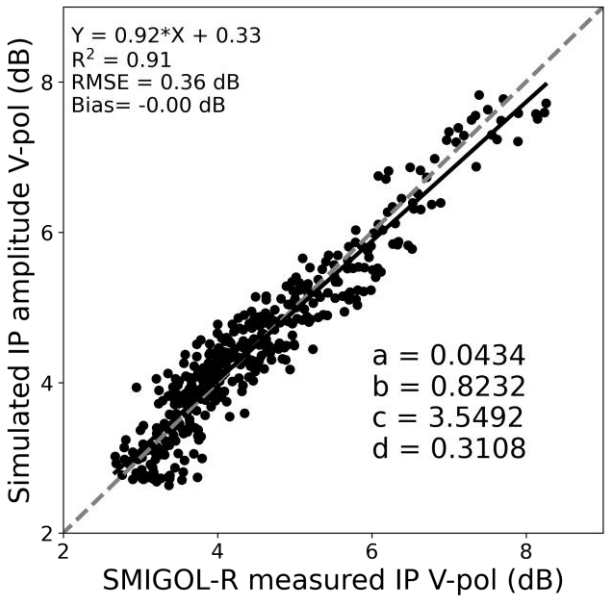

Fig. 5. Simulated IP at V-pol from the calibrated empirical model (2) against measured IP by the SMIGOL-R. The simulation was performed on the validation dataset.

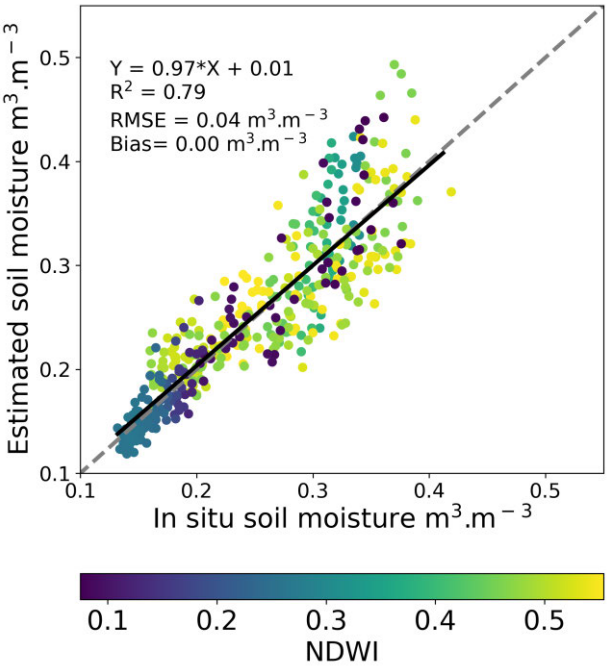

Fig. 6. Estimated SM from the calibrated empirical model [see (2)] against in situ SM. The simulation was performed on the validation dataset.

To summarize, the analysis of the experimental data shows that the L-band IP amplitude at V-pol is sensitive to the SM even when the grass-related NDWI is at a maximum. Moreover, the results showed that the sensitivity of IP amplitude to SM decreases with NDWI increasing due to the attenuation of IP amplitude by the grass water content. Therefore, in order to estimate the SM with good accuracy, the vegetation contribution to the IP amplitude must be considered. Importantly, the analysis of the experimental data confirms that the proposed empirical equation [see (2)] can be used to describe the variation of IP according to SM and NDWI. The results are in line with those obtained from the study by [21], where data from GNSS-R and optical imagery from the moderate resolution imaging spectroradiometer (MODIS) satellite were used to assess the sensitivity of GNSS-R reflectivity to SM and vegetation over different types of surfaces (forest, shrubs, savanna, and grassland). The results showed that as the NDVI increases (i.e., vegetation cover increases), the sensitivity of GNSS-R reflectivity to SM decreases because the vegetation layer attenuates the GPS signal. The results also showed that the sensitivity of GNSS-R reflectivity to SM remains significant at higher NDWI values.

B. Empirical Model Calibration and SM Estimation

The empirical model [see (2)] was calibrated to estimate SM from the IP amplitude. Fig. 5 shows that the estimated IP amplitude from the calibrated model accurately simulates the measured IP amplitude in the validation dataset (RMSE = 0.36 dB, Bias = 0 dB, and $R^2 = 0.91$), indicating that the empirical model [see (2)] indeed describes the actual variations of IP amplitude according to SM and NDWI variations. In addition, the SM was estimated from the validation dataset by inverting the calibrated empirical model. In this case, the results show that the calibrated model provides a nonbiased estimation of SM with an RMSE = 0.04 $m^3 \cdot m^{-3}$ and an $R^2 = 0.79$ (Fig. 6). Furthermore, Fig. 6 shows that the accuracy of SM estimation is higher when NDWI is low. For instance, for NDWI < 0.3, the RMSE of estimated SM was 0.03 $m^3 \cdot m^{-3}$, whereas for NDWI higher than 0.3, the RMSE was 0.05 $m^3 \cdot m^{-3}$. The model calibration and validation were performed for all available GPS satellites, with no outliers observed that could be attributed to specific GPS transmitters. The sensor works with a differential signal and a difference in the transmitter power should not affect the results.

The estimated calibration parameters with the optimization shows that the scattered contribution of SM (c = 3.5492) is more important than that of the vegetation (a = 0.0434), with the vegetation contribution playing more of a role in attenuating the IP amplitude (b = 0.8232). Therefore, in the

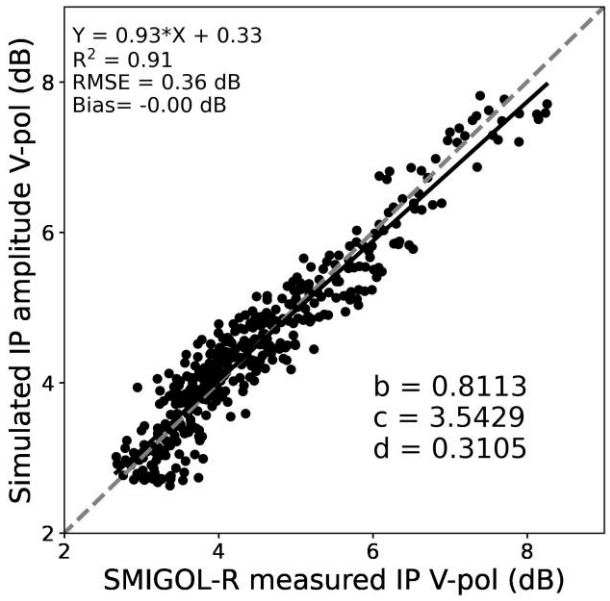

Fig. 7. Simulated IP at V-pol from the calibrated empirical model [see (3)] against measured IP at V-pol by the SMIGOL-R. The simulation was performed on the validation dataset.

absence of an enhanced contribution from the vegetation layer on the IP amplitude, the scattered contribution of vegetation in (2) $[a * \text{NDWI} * (1 - e^{-b*\text{NDWI}})]$ can be ignored. In that case, (2) can be simplified via (3), where the IP amplitude is expressed only as a function of the scattered contribution of SM attenuated by the vegetation layer as follows:

$$A = c * \text{SM}^d * e^{-b*\text{NDWI}}. \tag{3}$$

Similar to (2), (3) was calibrated (i.e., estimating c, d, and b) to estimate the SM while considering only the attenuation effects caused by the vegetation on the IP amplitude. The comparison of simulated IP amplitudes with those measured by the SMIGOL-R (validation dataset) shows that (3) explains the behavior of the IP amplitude in relation to SM and the vegetation layer with an accuracy (RMSE = 0.39 dB and $R^2 = 0.89$) similar to that obtained using (2) (Figs. 6 and 7). This indicates that the enhanced vegetation contribution to the IP amplitude (scattered contribution of vegetation) is either not present or very weak (Figs. 5 and 7). The achieved accuracy of estimated SM with the calibrated (3) was similar to that obtained with (2) (nonbiased estimation with RMSE = 0.04 $\text{m}^3 \cdot \text{m}^{-3}$). Fig. 8 shows that the estimated SM derived from (3) covary with the temporal variation of in situ SM. Therefore, ignoring the scattered contribution of grassland $[a * \text{NDWI}]$ to IP at V-pol will not deteriorate the SM estimation accuracy.

The simplified empirical model [see (3)] provides an interesting opportunity to estimate the NDWI if the SM is known from an independent source, such as a colocated permanent in situ sensor. Indeed, in contrast to (2), (3) can be numerically resolved to estimate the NDWI. To explore this, (3) was used to estimate the NDWI using the GNSS-R observations and in situ SM in the validation dataset as inputs. The estimated NDWI was then compared to the Sentinel-2 data, with the results delivering a high estimation accuracy (RMSE = 0.05

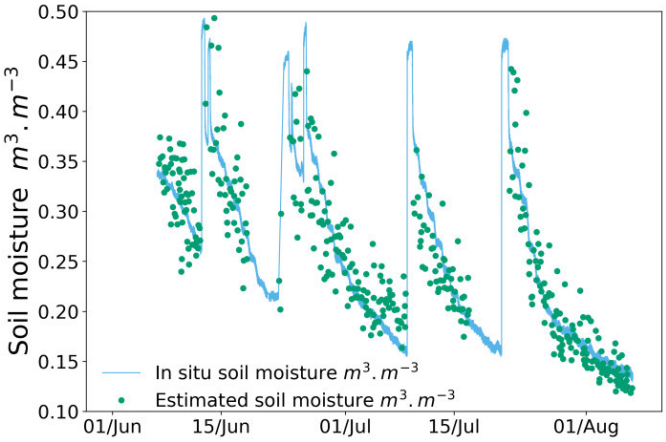

Fig. 8. Temporal variations of in situ SM and estimated SM based on (3).

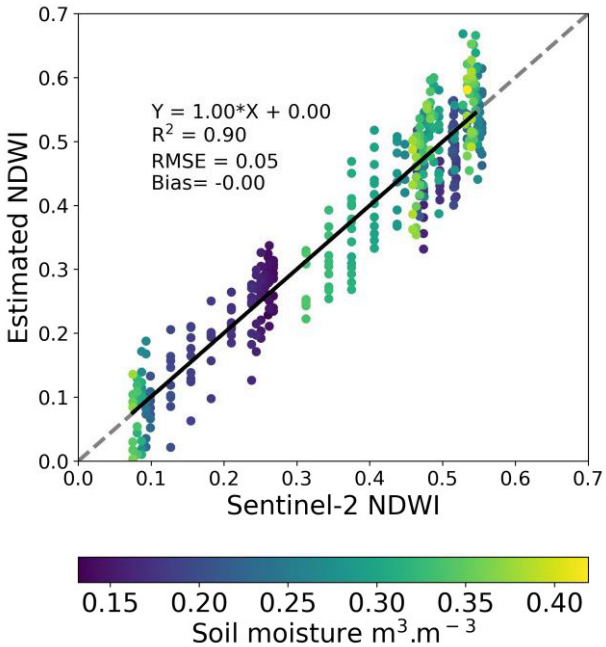

Fig. 9. Estimated NDWI against NDWI from Sentinel-2. The estimation of NDWI was performed using the calibrated simplified empirical model (3).

and an $R^2 = 0.90$), indicating that the variation in IP attenuation due to vegetation growth can be used to infer the NDWI, which may serve as a potential proxy for biomass (Fig. 9). Having repetitive NDWI or SM estimation over a plot may also help in calibrating crop models, providing a tool for irrigation optimization that can be applied to improve crop management at the farm scale. Furthermore, applying the method developed herein using GNSS-R reflectivity from satellites (such as Spire GNSS-R) that is attenuated by the vegetation layer [21] and independent SM products from satellites such as SM and ocean salinity (SMOS) and SM active passive (SMAP) may provide an avenue to infer a proxy of biomass at a global scale.

V. Challenges and Limitations

An experiment to estimate SM using IP amplitude was conducted over an irrigated grassland field in which the vegetation height reached up to 90 cm before harvest. The

IP amplitude was modeled as a function of SM at 7 cm depth and NDWI, using an empirical approach that does not include parameters affecting the IP amplitude, such as the antenna height and the incidence angle. Additionally, it uses NDWI, which does not account for all vegetation parameters contributing to the GNSS-R reflected signals, particularly vegetation structure [15]. Furthermore, the proposed model (2) and (3) does not include a parameter to account for roughness scattering, as the plot roughness remained unchanged during the experiment. Consequently, the empirical model (2) and (3) calibrated herein is site-specific, and hence, for other sites, it would require the addition of a term to account for the roughness scattering contribution to the IP amplitude recorded by the SMIGOL-R. It is worth mentioning that the NDWI may saturate before the grass reaches its maximum level of water content, which may lead to an inaccurate representation of the water status and decrease the SM accuracy for high vegetation water content values. The results obtained in this study (nonsignificant scattered contribution of vegetation and high SM estimation accuracy) are expected to be applicable to crops with plant morphology similar to grassland (e.g., wheat and barley). For vegetation with more complex morphology and/or larger element sizes, such as sunflowers and maize, it is expected that the canopy would yield a significant scattered contribution to the GNSS-R reflected signal [26]. For heterogeneous vegetated areas such as forests, it is almost certain that the empirical model developed herein would be unable to retrieve SM and a biomass proxy, at least with sufficient accuracy, due to the expected high contribution of tree trunks and branches, which can be highly variable. To address these limitations, an experiment is currently being conducted in a super high-density olive orchard, and another experiment is planned over different crop fields with more complex morphology and larger crop elements.

The model developed herein uses the IP amplitude, which is estimated from IP oscillations for elevation angles between 20° and 40°. Therefore, IP oscillations corresponding to different Fresnel zones were combined to provide an SM estimation. Accordingly, our approach precludes the possibility of SM mapping within the GNSS footprint because the IP amplitude cannot be assigned to specific satellite elevation and azimuth values (i.e., given the Fresnel zone and specular point coordinates).

The synergistic use of IP amplitude and Sentinel-2 derived NDWI in an empirical model for SM estimation shows satisfactory results for continuous monitoring of SM at 7 cm depths. However, root zone SM is also a vital variable needed in hydrological applications. Leveraging previous studies exploring SM profile extrapolation, GNSS-R-derived SM could be used to estimate root zone moisture via an exponential filter [27] or by assimilating GNSS-R-derived surface SM into a hydrological model [28]. Additionally, further studies should explore the potential of GNSS-R L band to estimate SM at shallower depths (<7 cm) [29].

VI. Conclusion

In this study, a method based on the use of IP amplitude was developed to practically estimate SM and NDWI over an irrigated grassland field. Results showed that the IP amplitude at V-pol, computed from the IP oscillation, is sensitive to SM, with sensitivity decreasing with vegetation development due to the attenuation by the vegetation layer. This behavior of the IP amplitude at V-pol was modeled with an empirical equation that was calibrated and shows high overall accuracy in SM estimation, delivering an RMSE of 0.04 $m^3 \cdot m^{-3}$. The estimation accuracy was higher for low vegetation conditions (NDWI $\leq$ 0.3), with an RMSE = 0.03 $m^3 \cdot m^{-3}$, compared to high vegetation conditions (NDWI $>$ 0.3), with an RMSE = 0.05 $m^3 \cdot m^{-3}$. Empirical model calibration results show that the vegetation layer attenuates the IP amplitude as the canopy layer develops with nonsignificant scattered contribution. This allows the development of a simple empirical model for estimating NDWI that is a proxy of fresh biomass [30] with high accuracy (RMSE = 0.05), in cases where the SM is known. Establishing a network of SMIGOL-R receivers across diverse ecosystems will enhance the accuracy of satellite-based missions aimed at tracking global SM.

References

[1] C. Corradini, "Soil moisture in the development of hydrological processes and its determination at different spatial scales," *J. Hydrol.*, vol. 516, pp. 1–5, Aug. 2014, doi: 10.1016/j.jhydrol.2014.02.051.

[2] W. L. Crosson, C. A. Laymon, R. Inguva, and M. P. Schamschula, "Assimilating remote sensing data in a surface flux–soil moisture model," *Hydrological Processes*, vol. 16, no. 8, pp. 1645–1662, Jun. 2002.

[3] C. P. Hung, B. Schalge, G. Baroni, H. Vereecken, and H. H. Franssen, "Assimilation of groundwater level and soil moisture data in an integrated land surface-subsurface model for Southwestern Germany," *Water Resour. Res.*, vol. 58, no. 6, p. 2021, Jun. 2022, doi: 10.1029/2021wr031549.

[4] C. Ma, X. Li, and M. F. McCabe, "Retrieval of high-resolution soil moisture through combination of Sentinel-1 and Sentinel-2 data," *Remote Sens.*, vol. 12, no. 14, p. 2303, Jul. 2020, doi: 10.3390/rs12142303.

[5] S. Millán, J. Casadesús, C. Campillo, J. Mo nino, and H. Prieto, "Using soil moisture sensors for automated irrigation scheduling in a plum crop," *Water*, vol. 11, no. 10, p. 2061, Oct. 2019, doi: 10.3390/w11102061.

[6] S. Paloscia, S. Pettinato, E. Santi, C. Notarnicola, L. Pasolli, and A. Reppucci, "Soil moisture mapping using Sentinel-1 images: Algorithm and preliminary validation," *Remote Sens. Environ.*, vol. 134, pp. 234–248, Jul. 2013.

[7] M. El Hajj, N. Baghdadi, and M. Zribi, "Comparative analysis of the accuracy of surface soil moisture estimation from the C- and L-bands," *Int. J. Appl. Earth Observ. Geoinf.*, vol. 82, Oct. 2019, Art. no. 101888.

[8] M. F. McCabe et al., "The future of Earth observation in hydrology," *Hydrol. Earth Syst. Sci.*, vol. 21, no. 7, pp. 3879–3914, Jul. 2017.

[9] K. M. Larson, E. E. Small, E. Gutmann, A. Bilich, P. Axelrad, and J. Braun, "Using GPS multipath to measure soil moisture fluctuations: Initial results," *GPS Solutions*, vol. 12, no. 3, pp. 173–177, Jul. 2008.

[10] C. C. Chew, E. E. Small, K. M. Larson, and V. U. Zavorotny, "Effects of near-surface soil moisture on GPS SNR data: Development of a retrieval algorithm for soil moisture," *IEEE Trans. Geosci. Remote Sens.*, vol. 52, no. 1, pp. 537–543, Jan. 2014.

[11] N. Rodriguez-Alvarez et al., "Soil moisture retrieval using GNSS-R techniques: Experimental results over a bare soil field," *IEEE Trans. Geosci. Remote Sens.*, vol. 47, no. 11, pp. 3616–3624, Nov. 2009.

[12] V. U. Zavorotny, K. M. Larson, J. J. Braun, E. E. Small, E. D. Gutmann, and A. L. Bilich, "A physical model for GPS multipath caused by land reflections: Toward bare soil moisture retrievals," *IEEE J. Sel. Topics Appl. Earth Observ. Remote Sens.*, vol. 3, no. 1, pp. 100–110, Mar. 2010.

[13] A. Alonso-Arroyo et al., "Improving the accuracy of soil moisture retrievals using the phase difference of the dual-polarization GNSS-R interference patterns," *IEEE Geosci. Remote Sens. Lett.*, vol. 11, no. 12, pp. 2090–2094, Dec. 2014.

[14] M. M. El Hajj et al., "Ground-based soil moisture retrieval using the correlation between dual-polarization GNSS-R interference patterns," *IEEE Trans. Geosci. Remote Sens.*, vol. 62, 2024, Art. no. 5800210, doi: 10.1109/TGRS.2023.3337841.
[15] N. Rodriguez-Alvarez et al., "Land geophysical parameters retrieval using the interference pattern GNSS-R technique," *IEEE Trans. Geosci. Remote Sens.*, vol. 49, no. 1, pp. 71–84, Jan. 2011, doi: 10.1109/TGRS.2010.2049023.
[16] G. Lérondel and R. Romestain, "Fresnel coefficients of a rough interface," *Appl. Phys. Lett.*, vol. 74, no. 19, pp. 2740–2742, May 1999.
[17] G. Rozenberg and A. Salomaa, *The Mathematical Theory of L Systems*. New York, NY, USA: Academic, 1980.
[18] A. Martinez-Vazquez, A. Camps, N. Duffo, M. Vall-Ilossera, and J. M. Lopez-Sanchez, "Full polarimetric emissivity of vegetation-covered soils: Vegetation structure effects," in *Proc. IEEE Int. Geosci. Remote Sens. Symp.*, vol. 6, Jun. 2002, pp. 3542–3544, doi: 10.1109/IGARSS.2002.1027242.
[19] M. Hajj et al., "Irrigated grassland monitoring using a time series of TerraSAR-X and COSMO-SkyMed X-band SAR data," *Remote Sens.*, vol. 6, no. 10, pp. 10002–10032, Oct. 2014, doi: 10.3390/rs61010002.
[20] S. Zhang et al., "Use of GNSS SNR data to retrieve soil moisture and vegetationvariables over a wheat crop," *Hydrol. Earth Syst. Sci.*, Mar. 2017, doi: 10.5194/hess-2017-152.
[21] A. Camps et al., "Sensitivity of GNSS-R spaceborne observations to soil moisture and vegetation," *IEEE J. Sel. Topics Appl. Earth Observ. Remote Sens.*, vol. 9, no. 10, pp. 4730–4742, Oct. 2016, doi: 10.1109/JSTARS.2016.2588467.
[22] C. C. Chew, E. E. Small, K. M. Larson, and V. U. Zavorotny, "Vegetation sensing using GPS-interferometric reflectometry: Theoretical effects of canopy parameters on signal-to-noise ratio data," *IEEE Trans. Geosci. Remote Sens.*, vol. 53, no. 5, pp. 2755–2764, May 2015, doi: 10.1109/TGRS.2014.2364513.
[23] B. C. Gao, "NDWI-A normalized difference water index for remote sensing of vegetation liquid water from space," *Remote Sens. Environ.*, vol. 58, no. 3, pp. 257–266, Dec. 1996, doi: 10.1016/S0034-4257(96)00067-3.
[24] D. Chen, J. Huang, and T. J. Jackson, "Vegetation water content estimation for corn and soybeans using spectral indices derived from MODIS near- and short-wave infrared bands," *Remote Sens. Environ.*, vol. 98, nos. 2–3, pp. 225–236, Oct. 2005, doi: 10.1016/j.rse.2005.07.008.
[25] S. Vey, A. Güntner, J. Wickert, T. Blume, and M. Ramatschi, "Long-term soil moisture dynamics derived from GNSS interferometric reflectometry: A case study for Sutherland, South Africa," *GPS Solutions*, vol. 20, no. 4, pp. 641–654, Oct. 2016, doi: 10.1007/s10291-015-0474-0.
[26] J. Paris, "The effect of leaf size on the microwave backscattering by corn," *Remote Sens. Environ.*, vol. 19, no. 1, pp. 81–95, Feb. 1986.
[27] Y. Yang et al., "An exponential filter model-based root-zone soil moisture estimation methodology from multiple datasets," *Remote Sens.*, vol. 14, no. 8, p. 1785, Apr. 2022.
[28] P. Heidary, L. Farhadi, and M. U. Altaf, "Estimation of root zone soil moisture profile by reduced-order variational data assimilation using near surface soil moisture observations," *IEEE J. Sel. Topics Appl. Earth Observ. Remote Sens.*, vol. 15, pp. 2394–2409, 2022.
[29] P. J. Shellito et al., "SMAP soil moisture drying more rapid than observed in situ following rainfall events," *Geophys. Res. Lett.*, vol. 43, no. 15, pp. 8068–8075, Aug. 2016, doi: 10.1002/2016gl069946.
[30] J. Serrano, S. Shahidian, and J. M. da Silva, "Evaluation of normalized difference water index as a tool for monitoring pasture seasonal and inter-annual variability in a Mediterranean Agro-Silvo-Pastoral system," *Water*, vol. 11, no. 1, p. 62, Jan. 2019, doi: 10.3390/w11010062.

Marcel M. El Hajj received the Ph.D. degree in geomatics and remote sensing from AgroParisTech University, Paris, France, in 2015.

He was a Research Engineer with the National Research Institute of Science and Technology for Environment and Agriculture, Villeneuve-d'Ascq, France. He worked as a Modeling Researcher with the Intelligence Technology Knowledge, Montpellier, France. He has been a Post-Doctoral Researcher with the King Abdullah University of Sciences and Technology, Thuwal, Saudi Arabia, since 2021. His main field of interest is the use of microwave, optical, and LiDAR remote sensing data for land surface applications.

Susan C. Steele-Dunne (Member, IEEE) received the S.M. and Ph.D. degrees in hydrology from Massachusetts Institute of Technology, Cambridge, MA, USA, in 2002 and 2006, respectively.

She has been with the Faculty of Civil Engineering and Geosciences, Delft University of Technology, Delft, The Netherlands, since 2008, where she is currently a Professor with the Department of Geoscience and Remote Sensing. She leads the M-WAVE Group, which performs research from field to global scales, combining in situ and spaceborne data to improve the understanding of microwave interactions with vegetation. Her research interests include data assimilation, modeling, and machine learning to exploit spaceborne radar instruments for applications in ecosystem and agricultural monitoring.

Kasper Johansen received the Ph.D. degree in remote sensing from the University of Queensland, Brisbane, QLD, Australia, in 2007.

Since 2017, he has been a Research Scientist with the King Abdullah University of Science and Technology, Thuwal, Saudi Arabia. His main research interests are focused on processing and analyzing high spatial resolution remotely sensed multispectral, hyperspectral, LiDAR, and thermal image data acquired from satellite, airborne, and UAV-based sensors to extract ecologically meaningful information.

Dr. Johansen is an Associate Editor of *Frontiers in Remote Sensing*.

Samer K. Almashharawi received the M.Sc. degree in environmental science and engineering from the King Abdullah University of Science and Technology, Thuwal, Saudi Arabia, in 2011.

He has been a Research Specialist with the King Abdullah University of Science and Technology, since 2012. His main fields of interest include the use of cosmic ray neutron sensors and in situ data for precision agriculture applications.

Oliver M. Lopez Valencia received the Ph.D. degree in environmental science and technology from the King Abdullah University of Science and Technology, Thuwal, Saudi Arabia, in 2018.

He has since worked as a Geospatial Data Scientist with the Hydrology, Agriculture, and Land Observation Research Group, Thuwal. His main field of interest is the use of satellite optical and thermal data for agricultural remote sensing applications including field mapping and water use estimation at regional to national scales.

Omar A. López Camargo (Student Member, IEEE) received the B.S. degree in electronic engineering from the National University of Colombia, Bogota, Colombia, in 2020, and the M.S. degree in environmental science and engineering from the King Abdullah University of Science and Technology (KAUST), Thuwal, Saudi Arabia, in 2022, where he is currently pursuing the Ph.D. degree in environmental science and engineering, with a primary focus on remote sensing.

His expertise lies in the utilization of agile robots, unmanned aerial vehicles (UAVs), and satellites for vegetation assessment, particularly in areas such as biodiversity mapping and climate change monitoring and mitigation.

Adria Amezaga-Sarries received the Ph.D. degree in ground-based synthetic aperture radar from the Universitat Politècnica de Catalunya, Barcelona, Spain, in 2020.

He was involved in GNSS Reflectometry and New Space research projects with the Universitat Politècnica de Catalunya. He is the Co-Founder of Microwave Sensors and Electronics SL (MWSE), where he leads mixed-signal, RF, and microwave design tasks for remote sensing applications, including spaceborne GNSS receivers, microwave radiometers, and ground-based radar systems. His main research interests include the application of multifrequency in ground-based synthetic aperture radar systems.

Andreu Mas-Viñolas received the bachelor's degree in aerospace engineering and telecommunications engineering from the Polytechnic University of Catalunya, Barcelona, Spain, in 2022, where he is currently pursuing the M.Sc. degree in telecommunications, specializing in remote sensing.

Since 2022, he has been working on the development of near-ground remote sensing systems with Microwave Sensors and Electronics Company, Barcelona. His main fields of interest include the development of remote sensing technologies to study the evolution of natural phenomena such as climate change.

Dominique Courault received the Ph.D. degree in soil sciences from Paris VI University, Paris, France, in 1989.

From 2007 to 2012, she was a member (elected) of the Scientific Council of PACA, and from 2013 to 2018, she was a member of the Scientific Committee of THEIA Land Data Center, providing free remote sensing products. From 2015 to 2020, she was also a member (nominated) of the Scientific Commission (CSS STEA) with INRA for a Scientist evaluation. From 2016 to 2020, she was a member (elected) of the Scientific Council of Environment and Agronomy Department, INRA, Paris. She has been a Scientist (DR2-HDR) and a Research Director with UMR 1114 EMMAH, Avignon, France; and INRAE Avignon, Avignon, since 1990. She used various models (SVAT and crop models) and different types of remote sensing data (AVHRR, Landsat, SPOT, Sentinel, and airborne sensors) to take into account the spatial variability of crops. She analyzes the impact of agricultural practices on yield variability in assimilating products derived from remote sensing. Since 2016, she has been co-managing the DREAM team, UMR EMMAH. Her scientific project is to develop tools based on modeling and remote sensing data for better water and crop management at a regional scale.

Claude Doussan received the Ph.D. degree in hydrogeology/hydrology from the École nationale supérieure des mines de Paris, Paris, France, in 1999.

He is currently a Researcher with INRAE, EMMAH Lab, Avignon, France. His research topics address soil–plant interactions, soil hydrology, and applications of geophysics for monitoring soil/plant properties, with a global focus on plant water use and tolerance to water deficit.

Matthew F. McCabe received the Ph.D. degree in civil and environmental engineering from the University of Newcastle, Callaghan, Australia, in 2003.

He is currently a Professor of remote sensing and water security and the Director of the KAUST Climate and Livability Initiative, King Abdullah University of Science and Technology, Thuwal, Saudi Arabia. His research explores a range of multidisciplinary issues around water and food security, climate change impacts, precision agriculture, and water resources monitoring and modeling.